Towards Individual Tone Preference in Underwater Image Enhancement

Xu Liu, *Student Member, IEEE*, Yang Zhao, *Member, IEEE*, Kaichen Chi,
Zhao Zhang, *Senior Member, IEEE*, Yanxiang Chen, Wei Jia, *Member, IEEE*

***Abstract*—Underwater images often suffer from severe color distortion due to the challenging imaging environment. Underwater image enhancement (UIE) techniques have been developed to recover clear images, laying the foundation for various underwater researches. However, existing UIE methods tend to produce fixed results without considering individual preferences for different color tones. And there is no dataset with ground truth in different tones. Therefore, we came up with the possibility of using the currently popular multi-modal methods to control the color tone of enhanced images. This paper proposes a method for generating underwater enhanced images with cold, warm, and normal tones using multi-modal information supervision (MM-UIE). Firstly, we leverage the relationship between text prompt and images to supervise the generation of cold or warm images. Additionally, we introduce a 6D color operator, which not only enhances the tone control of underwater images but also serves as a bridge between different tone images. Finally, we also found that multimodal supervision methods can not only control the color tone of underwater images, but also improve the quality of underwater image generation. Experimental results demonstrate the superior performance of our method compared to state-of-the-art (SOTA) techniques. Our codes will be publicly available at: https://github.com/perseveranceLX/MM-UIE.**

***Index Terms*—Underwater image enhancement, multi-modal learning, 6D color operator, application of the large-scale generative model**

I. Introduction

Underwater images play an essential role in presenting oceanic information, offering a unique perspective to observe the wonders of the underwater world [1]–[3]. These images can provide information of organisms, terrains, and environmental conditions in the ocean, contributing to the protection and management of marine resources [4]–[8]. In addition, underwater images can also be used in fields such as scientific research, military reconnaissance, and entertainment, bringing enormous value and significance to humanity. However, underwater images often suffer from degradation issues such as color distortion, low contrast, and blurry details due to the complex and challenging imaging environments.

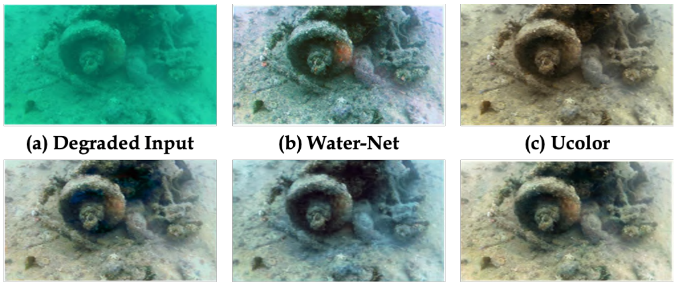

Fig. 1. Visual comparison of the (a) degraded input; (b) Water-Net; (c) Ucolor; (d) ours-normal; (e) ours-cold; (f) ours-warm in the UIEB dataset.

Underwater image enhancement and restoration aim to improve the visual quality of degraded underwater images. The current algorithms generate different styles of enhancement results as shown in Fig. 1: (b) Water-Net [9]; (c) Ucolor [10]. For example, the results of Water-Net tend to be cooler, while those of Ucolor tend to be warmer. People who prefer cooler colors are more likely to prefer the results provided by Water-Net. On the other hand, people who are drawn to warmer colors tend to favor the results that Ucolor produces. However, current underwater image enhancement algorithms [9]–[11] often overlook the subjective preferences and emotional responses of people towards the enhanced images.

Indeed, people have different color preferences due to personality variations, cultural background, and emotional experiences, which influence their feelings towards colors. For example, some people may prefer bright and vibrant colors like red, orange, and yellow as they evoke the sense of pleasure and excitement. Others may lean towards soft and elegant colors such as blue, green, and purple, which lead to a feeling of calmness and relaxation. With the advancements in large models and multimodal algorithms, learning-driven image enhancement algorithms can also leverage useful information from other modalities. Therefore, we propose an underwater image enhancement algorithm based on multimodal information supervision, which breaks the dilemma of requiring complete paired dataset supervision (as there is currently no dataset with different tone ground truth).

As shown in Fig. 2, our proposed method consists of two parts: color enhancement, which corrects the color of degraded underwater images, and detail enhancement, which restores the texture details of degraded images. Both text and image information are utilized to supervise the generation of enhanced underwater images with cool and warm tones. Additionally, It also illustrates the results of different tones generated by the proposed method. The contributions of this article are summarized as follows:

- ▶ We propose a method called Multi-Modal supervised

This work is supported by the Fundamental Research Funds for the Central Universities (No. JZ2022HGPA0309), the National Natural Science Foundation of China (No. 62272142, 62076086, 62472137, 62476077, 61972127) and Anhui Provincial Natural Science Fund for the Distinguished Young Scholars (No. 2008085J30). *(Corresponding author: Yang Zhao.)*

Xu Liu, Yang Zhao, Zhao Zhang, Yanxiang Chen and Wei Jia are with the School of Computer Science and Information Engineering, Hefei University of Technology, Hefei 230601, China (e-mail: dalong.xu.liu@ieee.org, yzhao@hfut.edu.cn, cszzhang@gmail.com, chenyx@hfut.edu.cn, jiawei@hfut.edu.cn).

Yang Zhao is also with Peng Cheng National Laboratory, Shenzhen 518000, China.

Kaichen Chi is with the School of Artificial Intelligence, Optics and Electronics (iOPEN), Northwestern Polytechnical University, Xi'an 710072, China (e-mail: chikaichen@mail.nwpu.edu.cn).

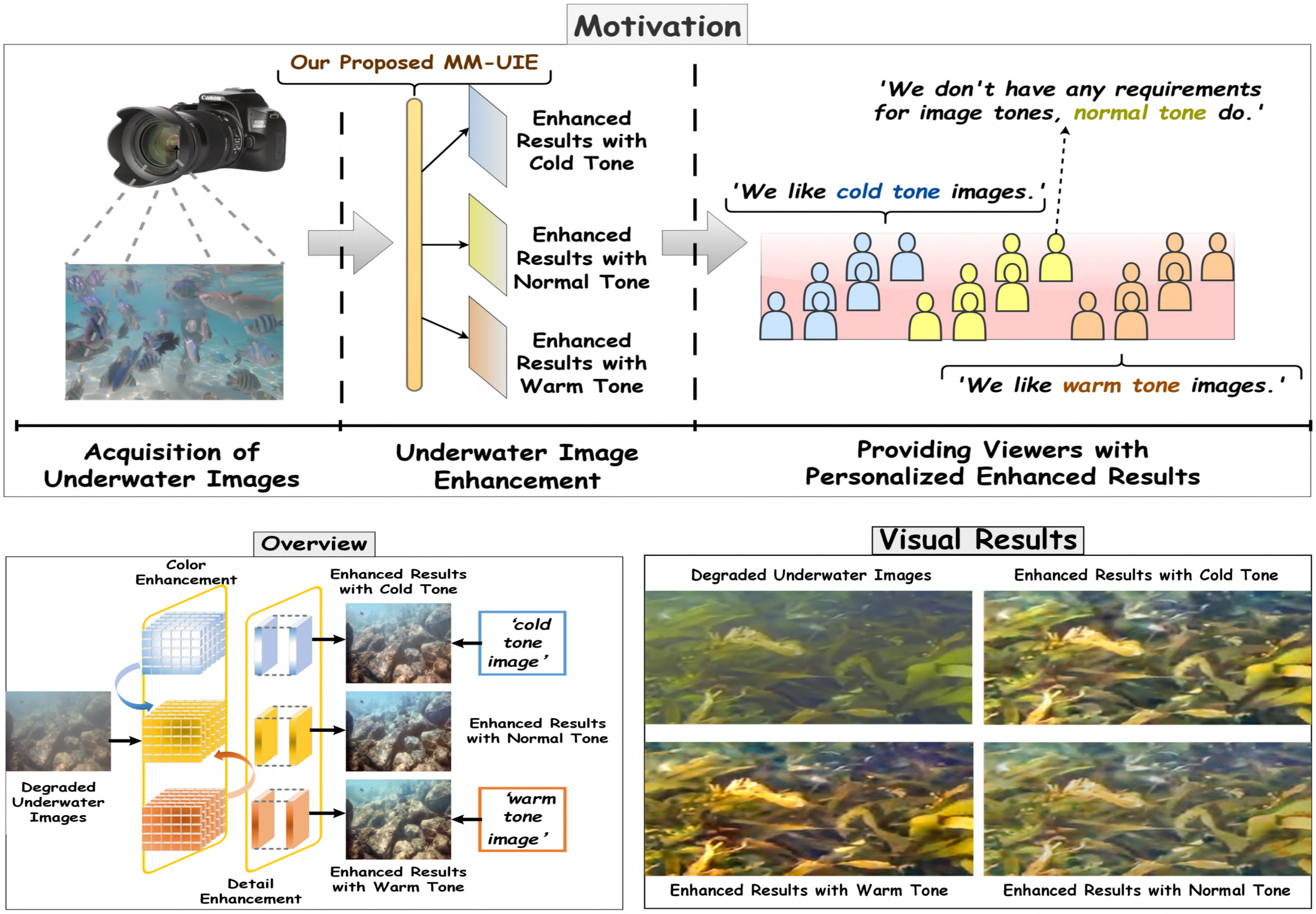
Motivation
Our Proposed MM-UIE
Enhanced Results with Cold Tone
Enhanced Results with Normal Tone
Enhanced Results with Warm Tone
'We don't have any requirements for image tones, normal tone do.'
'We like cold tone images.'
'We like warm tone images.'
Acquisition of Underwater Images
Underwater Image Enhancement
Providing Viewers with Personalized Enhanced Results
Overview
Color Enhancement
Enhanced Results with Cold Tone
'cold tone image'
Enhanced Results with Normal Tone
Degraded Underwater Images
'warm tone image'
Enhanced Results with Warm Tone
Detail Enhancement
Visual Results
Degraded Underwater Images
Enhanced Results with Cold Tone
Enhanced Results with Warm Tone
Enhanced Results with Normal Tone

Fig. 2. Demonstration of the motivation, overview and visual results of our proposed MM-UIE. Humans possess a unique ability to perceive color. We can observe in our daily lives that some people prefer cool tones, while others prefer warm tones, and some are unconcerned with tones at all. **Thus, as a task of underwater image enhancement (UIE), is it possible to generate enhanced images with different tones based on individual preferences?**

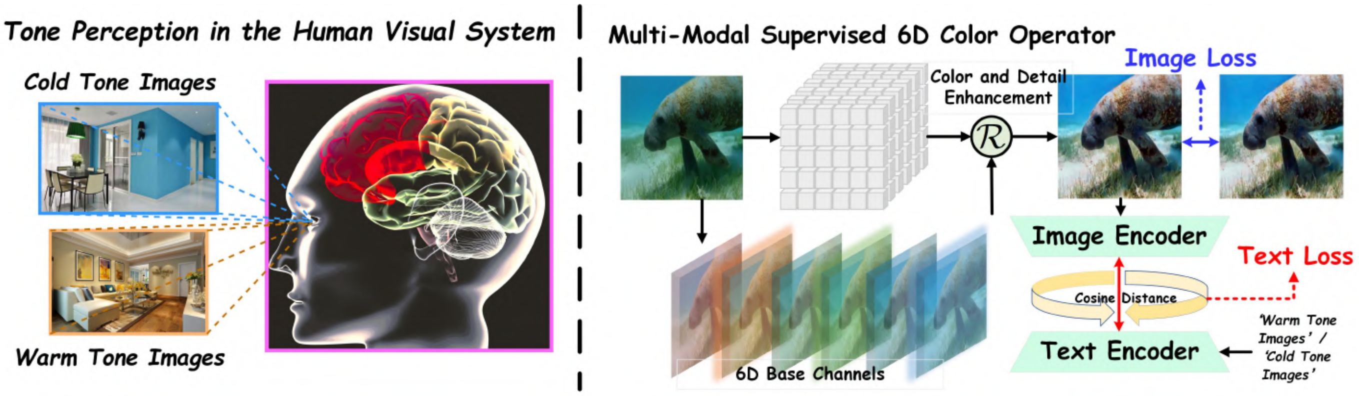
Tone Perception in the Human Visual System
Cold Tone Images
Warm Tone Images
Multi-Modal Supervised 6D Color Operator
Color and Detail Enhancement
$\mathcal{R}$
Image Loss
Image Encoder
Text Loss
Cosine Distance
Text Encoder
'Warm Tone Images' / 'Cold Tone Images'
6D Base Channels

Fig. 3. Tone perception in the human visual system vs. multi-modal supervised 6D color operator.

6D color operator for Underwater Image Enhancement (MM-UIE) in Fig. 3, which is the first method to achieve personalized UIE. By incorporating multi-modal information supervision and a 6D color operator, our method is pleasing to human visual system and generates enhanced images with three different tones according to the preferences of different populations.

- To control the color tone of the generated image, this paper proposes a novel cross-modal interaction method. To the best of our knowledge, this method is also the first multimodal approach in the UIE field. We design a loss function for supervised learning by calculating the cosine distance between two modal features.
- Color cast is a significant problem in underwater images. To address this issue and enhance the hue of the generated images, we propose a 6D color operator based on bilateral learning. This operator enables full-size color adjustment on the input image through six channel dimensions.
- Comprehensive subjective and objective experiments demonstrate that the proposed method effectively enhances underwater images, obtains better colors and fewer hazing artifacts, and exhibits clear advantages over other SOTA algorithms.

II. Related Work

This section will introduce works related to the algorithm proposed in this article. First, we will introduce the application scenario of underwater image enhancement and restoration and demonstrate some representative methods. Then, we will introduce the core of this article multi-modal information supervision and summarize how current enhancement algorithms apply multi-modal means.

A. Underwater Image Enhancement

Existing underwater image enhancement (UIE) algorithms can be roughly divided into three types, i.e., prior-based, physical-model-based, and learning-based methods.

Prior-based and physical models-based methods are traditional approaches. Prior-based methods tend to directly adjust the pixel values of the input image. For example, Ancuti *et al.* [12] design a novel white balance and fusion model, incorporating red channel priors and grayscale world assumptions for white balance. Zhang *et al.* [13] perform color correction based on histogram priors and combine it with contrast enhancement to emphasize details. Physical-model-based methods are often performed by solving imaging models. Song *et al.* [14] recover underwater images based on underwater optical imaging models and propose a dark channel prior model suitable for underwater scenes. Zhuang *et al.* [15] use hyper Laplacian reflection priors for the retinex variational model, combining priors and physical models. In order to enhance underwater polarization images, Shen *et al.* [16] present a polarization-driven method, which improves the contrast of underwater images, and they create a comprehensive benchmark for underwater polarization images. Although these traditional methods work well in some specific degraded images, for a large number of uncertainly degraded underwater images, these traditional algorithms are less robust, the enhancement effect is unstable, and some images still have color casts, artifacts, etc.

In recent years, learning-based image enhancement algorithms have become mainstream [17]–[21]. Learning-based UIE methods can be mainly divided into two types: convolutional neural networks (CNN)-based [9], [10], [22] and generative adversarial networks (GAN)-based [11], [23]–[25] methods. Learning-based methods learn the mapping from degraded images to clear images end-to-end, without the need for prior or physical models. UWCNN [26] is the first data-driven model, but its results exhibit severe color cast due to complete training based on synthetic datasets. Li *et al.* [9] fused the three enhanced results of traditional algorithms (i.e., white balance, gamma correction, and histogram equalization) through deep neural networks, resulting in fine visual quality. They also proposed Ucolor [10], which utilizes different color spaces for collaborative enhancement. To generate visually pleasure results, FUnIE-GAN [23] is based on conditional GAN and considers global similarity and content consistency through loss functions. As for polarization images, the U2PNet [27] proposes an unsupervised restoration method that analyzes the relationship between the transmission map and the degree of polarization. By incorporating intensity ratio constraints, the loss function preserves details and colors in the image. However, most current models rely on ground truth (GT) for learning, and their enhanced images neglect people's preferences, such as some people liking cold tone images while others liking warm tone images. Furthermore, most algorithms utilize a deep unrolling-based architecture that results in a greater number of parameters and a slower testing speed caused by multiple iterations.

B. Application of Multi-Modal Information

With the advent of large models, cross-modal learning has gained widespread attention, particularly between vision and text. The CLIP model [28] is a multimodal model based on contrastive learning, which can learn the matching relationship between text and image pairs. Recently, many works have applied CLIP models for supervised learning of images and videos. For example, Yang *et al.* [29] use text prompts as priors to enhance low-light images, resulting in visually pleasing results. Ju *et al.* [30] unify multiple tasks by adding a set of learnable vectors to the image-based visual multi-modal model. Liang *et al.* [31] propose a backlight image enhancement training scheme combined with the CLIP model: Image and text encoders using pre-trained CLIPs encode backlit and well-illuminated images, as well as learnable cue pairs (positive and negative samples) into the latent space.

Tone perception is an advanced function of the human visual system. To achieve enhanced results with different tones, we have come up with the idea of using text information to supervise learning through multi-modal models. Moreover, due to the U-Net baseline for generating the 6D color operators, our network is lightweight when compared with deep rolling-based models.

III. Methodology

The proposed MM-UIE consists of two stages, i.e., color enhancement and detail enhancement. In this section, we will introduce these two stages and the proposed loss function for cross-modality interactive constraint.

A. Multi-Modal Information for Tone Control

Underwater image enhancement (UIE) is a challenging task, and most of the enhancement results are unidirectional. **It is important to determine whether our enhanced images meet the preferences of our users.** Based on this motivation, we have designed a novel UIE algorithm that can generate different tones. Enhanced images with warm and normal tones to meet user preferences.

Current UIE dataset lacks GT with multiple tones. Therefore, we utilize a pre-trained CLIP [28] model for cross modal interaction, which can establish a connection between texts and images in the feature domain.

Given different tone enhanced results as $\mathcal{Y}_{\text{col}}$ and $\mathcal{Y}_{\text{war}}$, we use the image encoder α_{img} to generate image features:

$$\mathcal{W}_{\text{col}}^{\text{img}} = \alpha_{\text{img}}(\mathcal{Y}_{\text{col}}), \mathcal{W}_{\text{war}}^{\text{img}} = \alpha_{\text{img}}(\mathcal{Y}_{\text{war}}), \tag{1}$$

And text encoder α_{img} for generate text features:

$$\mathcal{W}_{\text{col}}^{\text{tex}} = \alpha_{\text{tex}}(\mathcal{Z}_{\text{col}}), \mathcal{W}_{\text{war}}^{\text{tex}} = \alpha_{\text{tex}}(\mathcal{Z}_{\text{war}}), \tag{2}$$

where we use the CLIP-RN50 baseline as the image and text encoder according to [29].

Hence, the loss function for tone control can be represented as follows:

$$\begin{aligned}\mathcal{L}^{\text{col}}_{\text{mm}}(\mathcal{W}^{\text{img}}_{\text{col}}, \mathcal{W}^{\text{tex}}_{\text{col}}) &= \frac{\left\langle \mathcal{W}^{\text{img}}_{\text{col}}, \mathcal{W}^{\text{tex}}_{\text{col}} \right\rangle}{\left\| \mathcal{W}^{\text{img}}_{\text{col}} \cdot \mathcal{W}^{\text{tex}}_{\text{col}} \right\|},\\ \mathcal{L}^{\text{war}}_{\text{mm}}(\mathcal{W}^{\text{img}}_{\text{war}}, \mathcal{W}^{\text{tex}}_{\text{war}}) &= \frac{\left\langle \mathcal{W}^{\text{img}}_{\text{war}}, \mathcal{W}^{\text{tex}}_{\text{war}} \right\rangle}{\left\| \mathcal{W}^{\text{img}}_{\text{war}} \cdot \mathcal{W}^{\text{tex}}_{\text{war}} \right\|},\end{aligned} \tag{3}$$

where $\langle , \rangle$ represents the cosine distance between two features, and $\|.\|$ means the L1 norm.

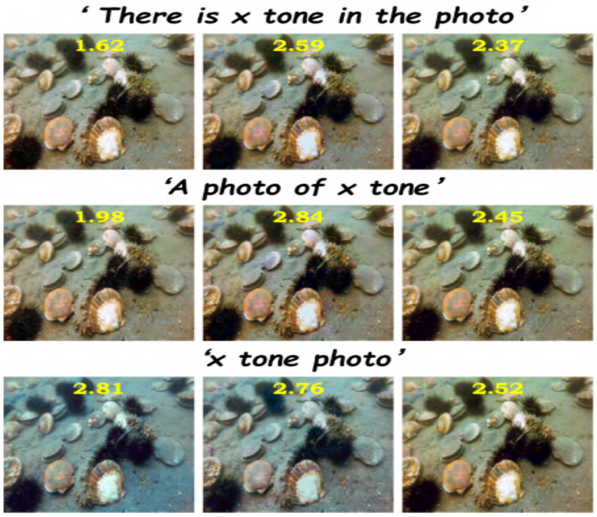

Fig. 4. Visual results comparison in different prompts. Scores range from 1 to 3, and the higher the score, the more appealing it will be to the viewer. From left to right x are 'cold', 'normal' and 'warm' respectively.

Influenced by [32], we use different text prompts for text tensor generation in Fig. 4. In order to find the feelings of different groups of people, we searched for 60 volunteers, including 20 volunteers who prefer cold tones and 20 volunteers who prefer warm tones. Then, the remaining 20 volunteers did not have a clear preference for color tones. The average score of each image is annotated in the Fig. 4. Obviously, when the prompt is 'x tone photo', the scores for each color tone are relatively balanced. Therefore, we choose this form as the prompts. In order to make the enhanced image quality, we also add the image loss. It includes $\mathcal{L}_1$ and $\mathcal{L}_{\text{VGG}}$ [10]:

$$\begin{aligned}\mathcal{L}^{1}_{\text{img}} &= \mathcal{L}_1(\mathcal{Y}_{\text{col}}, \mathcal{Y}_{\text{gt}}) + \mathcal{L}_1(\mathcal{Y}_{\text{nor}}, \mathcal{Y}_{\text{gt}})\\ &+ \mathcal{L}_1(\mathcal{Y}_{\text{war}}, \mathcal{Y}_{\text{gt}})\\ \mathcal{L}^{\text{VGG}}_{\text{img}} &= \mathcal{L}_{\text{VGG}}(\mathcal{Y}_{\text{col}}, \mathcal{Y}_{\text{gt}}) + \mathcal{L}_{\text{VGG}}(\mathcal{Y}_{\text{nor}}, \mathcal{Y}_{\text{gt}})\\ &+ \mathcal{L}_{\text{VGG}}(\mathcal{Y}_{\text{war}}, \mathcal{Y}_{\text{gt}})\end{aligned} \tag{4}$$

Hence, the total loss are as follows:

$$\begin{aligned}\mathcal{L}_{\text{tex}} &= \mathcal{L}^{\text{col}}_{\text{mm}}(\mathcal{W}^{\text{img}}_{\text{col}}, \mathcal{W}^{\text{tex}}_{\text{col}}) + \mathcal{L}^{\text{war}}_{\text{mm}}(\mathcal{W}^{\text{img}}_{\text{war}}, \mathcal{W}^{\text{tex}}_{\text{war}}),\\ \mathcal{L}_{\text{total}} &= \lambda_a \cdot \mathcal{L}^{1}_{\text{img}} + \lambda_b \cdot \mathcal{L}^{\text{VGG}}_{\text{img}} + \lambda_c \cdot \mathcal{L}_{\text{tex}}\end{aligned} \tag{5}$$

where λ_a, λ_b, and λ_c are three weights set to 3, 0.15, and 0.01, respectively.

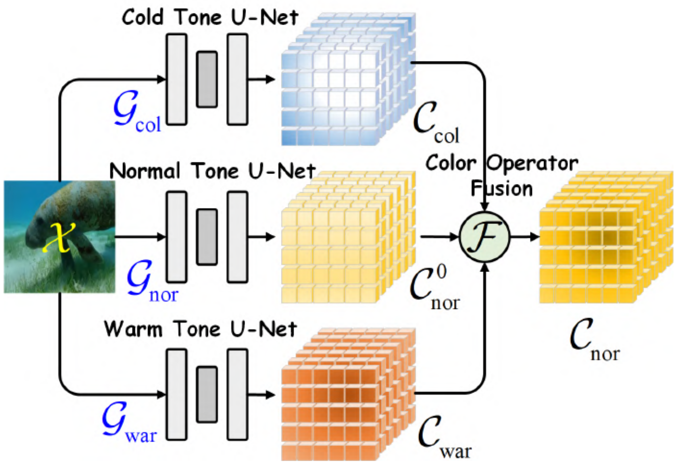
Cold Tone U-Net
$\mathcal{G}_{\text{col}}$
$\mathcal{C}_{\text{col}}$
Color Operator Fusion
Normal Tone U-Net
$\mathcal{X}$
$\mathcal{G}_{\text{nor}}$
$\mathcal{C}^0_{\text{nor}}$
$\mathcal{F}$
$\mathcal{C}_{\text{nor}}$
Warm Tone U-Net
$\mathcal{G}_{\text{war}}$
$\mathcal{C}_{\text{war}}$

Fig. 5. Generation process of the 6D color operator.

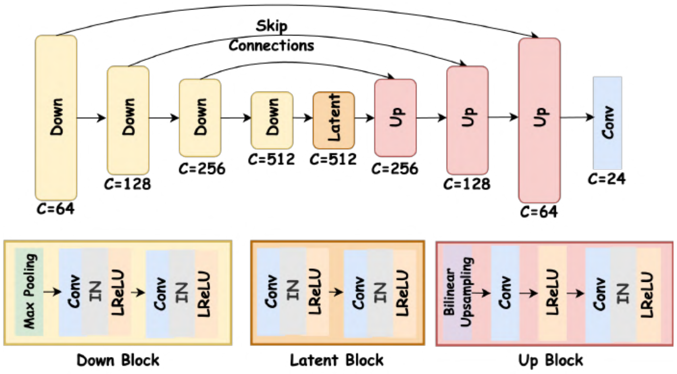

Fig. 6. Detailed diagram of the cold tone U-Net, normal tone U-Net and warm tone U-Net, C represents the number of channels. Conv denotes the convolutional layer. LReLU represents the leaky ReLU function, IN is the instance normalization.

TABLE I
MEMORY USAGE COMPARISON OF DIFFERENT BLOCKS (THE IMAGE SIZE IS 256 × 256). UP, LATENT AND DOWN REPRESENT THE UP BLOCK, LATENT BLOCK AND DOWN BLOCK, RESPECTIVELY.

U-Net Model	Memory Usage	
	Training↓	**Testing↓**
3 Down + 1 Latent + 2 Up	2161M	1929M
4 Down + 1 Latent + 3 Up	3432M	3282M
5 Down + 1 Latent + 4 Up	4338M	4017M

B. Color Enhancement

In this paper, a 6D color operator is designed to achieve color enhancement. Efficient bilateral learning model, which has been successfully applied for related tasks such as image dehazing [33]. However, due to the severe degradation of underwater images and the scattered distribution of degradation at different pixel points, traditional bilateral learning cannot handle the various and complex color distortions. Therefore, we propose a full-size 6D color operator, which can capture the color adjustment operator of the entire underwater image.

Given a degraded underwater image $\mathcal{X}$ composed of R, G, B three channels. In order to express the information of the original image more completely and enhance color effectively, we have modified the original RGB three channels as follows,

$$\begin{bmatrix} R' \\ G' \\ B' \end{bmatrix} = \mathcal{S} \cdot \begin{bmatrix} R \\ G \\ B \end{bmatrix}, \mathcal{S} = \begin{bmatrix} M & 0 & 0 \\ 0 & N & 0 \\ 0 & 0 & P \end{bmatrix}, \tag{6}$$

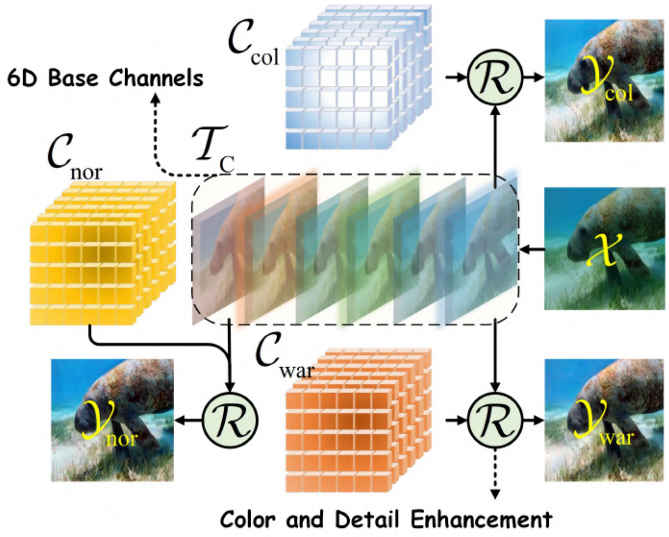
6D Base Channels
$\mathcal{C}_{\text{col}}$
$\mathcal{T}_{\text{C}}$
$\mathcal{C}_{\text{nor}}$
$\mathcal{X}$
$\mathcal{C}_{\text{war}}$
$\mathcal{R}$
$\mathcal{Y}_{\text{col}}$
$\mathcal{Y}_{\text{nor}}$
$\mathcal{Y}_{\text{war}}$
Color and Detail Enhancement

Fig. 7. Demonstration of different tone image generation.

where R', G', B' denote transformed RGB channels, and $\mathcal{S}$ represents a mapping diagonal matrix with three rows and three columns. Then, the Eq. (6) can be rewritten as follows:

$$\begin{aligned}\begin{bmatrix} R' \\ G' \\ B' \end{bmatrix} &= \begin{bmatrix} M & 0 & 0 \\ 0 & N & 0 \\ 0 & 0 & P \end{bmatrix} \cdot \begin{bmatrix} R \\ G \\ B \end{bmatrix} \\ &= \begin{bmatrix} M-1 & 0 & 0 \\ 0 & N-1 & 0 \\ 0 & 0 & P-1 \end{bmatrix} \cdot \begin{bmatrix} R \\ G \\ B \end{bmatrix} + \begin{bmatrix} R \\ G \\ B \end{bmatrix} \\ &= \mathcal{S}' \cdot \begin{bmatrix} R \\ G \\ B \end{bmatrix} + \begin{bmatrix} R \\ G \\ B \end{bmatrix}, \end{aligned} \tag{7}$$

where $\mathcal{S}'$ denotes generalized matrix from $\mathcal{S}$. The result is similar to $y = f(x) + x$, so we use a convolutional layer $\mathcal{U}$ and a residual connection for simulating the color transformation process as:

$$\mathcal{X}' = \mathcal{U}(\mathcal{X}) + \mathcal{X}, \mathcal{X} \in \begin{bmatrix} R \\ G \\ B \end{bmatrix}, \mathcal{X}' \in \begin{bmatrix} R' \\ G' \\ B' \end{bmatrix} \tag{8}$$

The original R, G, B and transformed R', G', B' are combined to six dimensions $\mathcal{T}_c$ for color adjustment, as follows,

$$\mathcal{T}_c \in \begin{bmatrix} R & R' & G & G' & B & B' \end{bmatrix}^T \tag{9}$$

In Fig. 5, we firstly use three U-Net to generate the 6D color operators for normal tone, cold tone, and warm tone, respectively:

$$\mathcal{C}_{\text{col}} = \mathcal{G}_{\text{col}}(\mathcal{X}), \mathcal{C}^0_{\text{nor}} = \mathcal{G}_{\text{nor}}(\mathcal{X}), \mathcal{C}_{\text{war}} = \mathcal{G}_{\text{war}}(\mathcal{X}), \tag{10}$$

where $\mathcal{G}_{\text{col}}$, $\mathcal{G}_{\text{nor}}$, and $\mathcal{G}_{\text{war}}$ denote cold-tone U-Net, normal-tone U-Net, and warm-tone U-Net, respectively, and $\mathcal{C}_{\text{col}}$, $\mathcal{C}^0_{\text{nor}}$ and $\mathcal{C}_{\text{war}}$ are generated 6D color operators. The detailed diagram of these three U-Net is shown in Fig. 6. Moreover, the Tab. I indicate the memory usage consumed by different blocks.

The Fig. 7 shows the generation process of different tone images. And the details of the color and detail enhancement is displayed in Fig. 8. The normal tone operator should well balance the warm and cold tones, we thus fuse three types of 6D operators to further improve the normal tone operator, as follows,

$$\mathcal{C}_{\text{nor}} = \mathcal{F}_{\text{ope}}(\mathcal{C}_{\text{col}}, \mathcal{C}^0_{\text{nor}}, \mathcal{C}_{\text{war}}), \tag{11}$$

which also confirms that the proposed 6D color operator can serve as a bridge connecting three different tones.

The main function of the operator fusion network $\mathcal{F}_{\text{ope}}$ is to fuse 6D color operators with three different tones ($\mathcal{C}_{\text{col}}$: the operator for the cold tone, $\mathcal{C}^0_{\text{nor}}$: the first operator for the normal tone and $\mathcal{C}_{\text{war}}$: the operator for the warm tone). Hence, we design a lightweight network $\mathcal{F}_{\text{ope}}$ to generate the final normal tone operator $\mathcal{C}_{\text{nor}}$. Through the operators for warm and cold tones and the first operator for the normal tone, the lightweight network $\mathcal{F}_{\text{ope}}$ can combine their respective excellent features and refine them in Fig. 9.

We use the affine function $\mathcal{A}$ to combine the operators and six channels for color enhancement:

$$\begin{aligned} \mathcal{V}_{\text{col}} = \mathcal{A} \cdot (\mathcal{C}_{\text{col}}, \mathcal{T}_c), \mathcal{V}_{\text{nor}} = \mathcal{A} \cdot (\mathcal{C}_{\text{nor}}, \mathcal{T}_c), \\ \mathcal{V}_{\text{war}} = \mathcal{A} \cdot (\mathcal{C}_{\text{war}}, \mathcal{T}_c), \end{aligned} \tag{12}$$

where $\mathcal{V}_{\text{col}}$, $\mathcal{V}_{\text{nor}}$ and $\mathcal{V}_{\text{war}}$ denote three features after color enhancement. Then the details of these operations: $\mathcal{A} \cdot (\mathcal{C}_{\text{col}}, \mathcal{T}_c)$; $\mathcal{A} \cdot (\mathcal{C}_{\text{war}}, \mathcal{T}_c)$; $\mathcal{A} \cdot (\mathcal{C}_{\text{nor}}, \mathcal{T}_c)$ are as follows:

$$\begin{aligned} \mathcal{A} \cdot (\mathcal{C}_{\text{col}}, \mathcal{T}_c) = \ \text{Cat} \Bigg(& \sum_{\eta_1 \in 1,2,3,4,5,6} \mathcal{C}^{\eta_1}_{\text{col}} \mathcal{T}_{\text{c}} + \mathcal{C}^7_{\text{col}}, \\ & \sum_{\eta_2 \in 8,9,10,11,12,13} \mathcal{C}^{\eta_2}_{\text{col}} \mathcal{T}_{\text{c}} + \mathcal{C}^{14}_{\text{col}}, \sum_{\eta_3 \in 15,16,17,18,19,20} \mathcal{C}^{\eta_3}_{\text{col}} \mathcal{T}_{\text{c}} + \mathcal{C}^{21}_{\text{col}} \Bigg) \end{aligned} \tag{13}$$

$$\begin{aligned} \mathcal{A} \cdot (\mathcal{C}_{\text{nor}}, \mathcal{T}_c) = \ \text{Cat} \Bigg(& \sum_{\eta_1 \in 1,2,3,4,5,6} \mathcal{C}^{\eta_1}_{\text{nor}} \mathcal{T}_{\text{c}} + \mathcal{C}^7_{\text{nor}}, \\ & \sum_{\eta_2 \in 8,9,10,11,12,13} \mathcal{C}^{\eta_2}_{\text{nor}} \mathcal{T}_{\text{c}} + \mathcal{C}^{14}_{\text{nor}}, \sum_{\eta_3 \in 15,16,17,18,19,20} \mathcal{C}^{\eta_3}_{\text{nor}} \mathcal{T}_{\text{c}} + \mathcal{C}^{21}_{\text{nor}} \Bigg) \end{aligned} \tag{14}$$

$$\begin{aligned} \mathcal{A} \cdot (\mathcal{C}_{\text{war}}, \mathcal{T}_c) = \ \text{Cat} \Bigg(& \sum_{\eta_1 \in 1,2,3,4,5,6} \mathcal{C}^{\eta_1}_{\text{war}} \mathcal{T}_{\text{c}} + \mathcal{C}^7_{\text{war}}, \\ & \sum_{\eta_1 \in 8,9,10,11,12,13} \mathcal{C}^{\eta_2}_{\text{war}} \mathcal{T}_{\text{c}} + \mathcal{C}^{14}_{\text{war}}, \sum_{\eta_1 \in 15,16,17,18,19,20} \mathcal{C}^{\eta_3}_{\text{war}} \mathcal{T}_{\text{c}} + \mathcal{C}^{21}_{\text{war}} \Bigg) \end{aligned} \tag{15}$$

where $\mathcal{C}_{\text{col/war/nor}} \in \mathbb{R}^{21 \times h \times w}$, $\mathcal{T}_{\text{c}} \in \mathbb{R}^{6 \times h \times w}$.

C. Detail Enhancement

The goal of detail enhancement is to restore information such as texture that has been degraded in the image, thereby improving the visual quality. We use the UIE model Boths [34] as the baseline to preliminarily enhance the details as:

$$\mathcal{E}_{\text{col}} = \mathcal{D}_{\text{col}}(\mathcal{X}), \mathcal{E}_{\text{nor}} = \mathcal{D}_{\text{nor}}(\mathcal{X}), \mathcal{E}_{\text{war}} = \mathcal{D}_{\text{war}}(\mathcal{X}), \tag{16}$$

where $\mathcal{E}_{\text{col}}$, $\mathcal{E}_{\text{nor}}$ and $\mathcal{E}_{\text{war}}$ denote results of three same detail enhancement baseline modules $\mathcal{D}_{\text{col}}$, $\mathcal{D}_{\text{nor}}$, and $\mathcal{D}_{\text{war}}$, as shown in Fig. 8. Then we concatenate the color enhancement feature

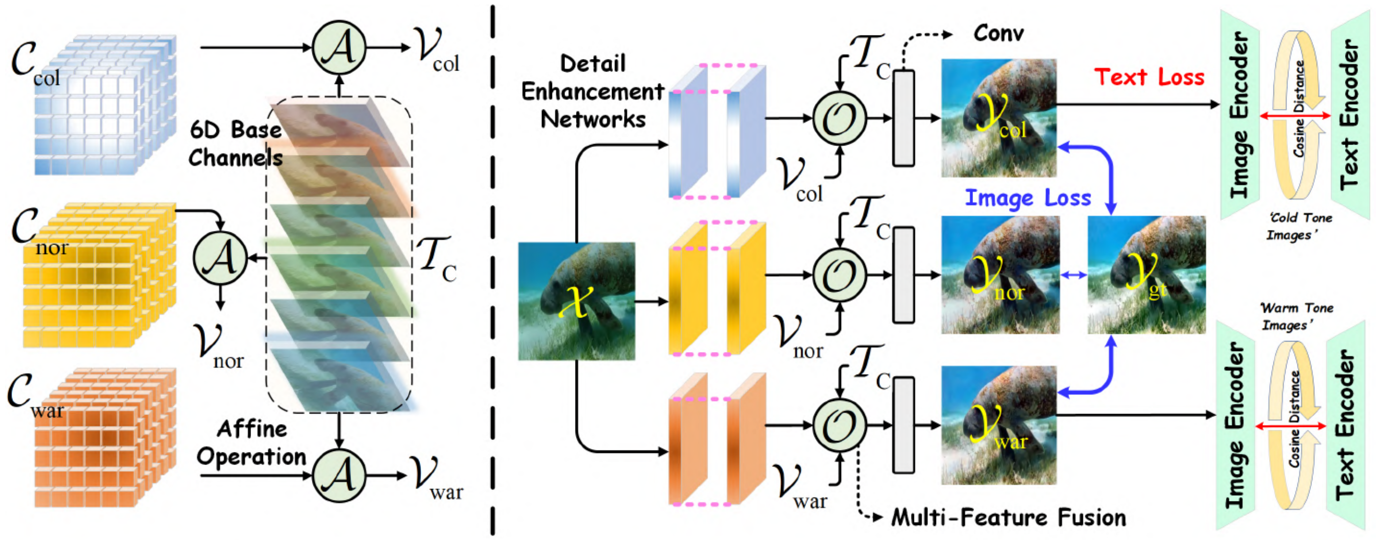
$\mathcal{C}_{\text{col}}$
$\mathcal{C}_{\text{nor}}$
$\mathcal{C}_{\text{war}}$
6D Base Channels
$\mathcal{T}_{\text{C}}$
Affine Operation
$\mathcal{A}$
$\mathcal{V}_{\text{col}}$
$\mathcal{V}_{\text{nor}}$
$\mathcal{V}_{\text{war}}$
Detail Enhancement Networks
$\mathcal{X}$
$\mathcal{O}$
Conv
Multi-Feature Fusion
$\mathcal{Y}_{\text{col}}$
$\mathcal{Y}_{\text{nor}}$
$\mathcal{Y}_{\text{war}}$
$\mathcal{Y}_{\text{gt}}$
Text Loss
Image Loss
Image Encoder
Text Encoder
Cosine Distance
'Cold Tone Images'
'Warm Tone Images'

Fig. 8. Indication of color (left) and detail (right) enhancement.

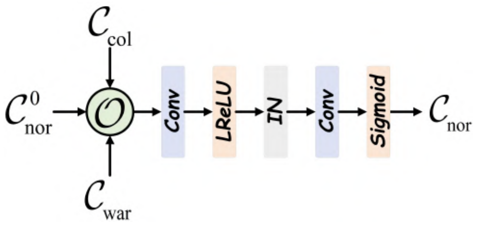
$\mathcal{C}_{\text{col}}$
$\mathcal{C}^0_{\text{nor}}$
$\mathcal{O}$
Conv
LReLU
IN
Conv
Sigmoid
$\mathcal{C}_{\text{nor}}$
$\mathcal{C}_{\text{war}}$

Fig. 9. Demonstration of the operator fusion network. Conv denotes the convolutional layer, LReLU and Sigmoid represent the leaky ReLU and sigmoid functions, IN is the instance normalization, $\mathcal{O}$ means the concatenation.

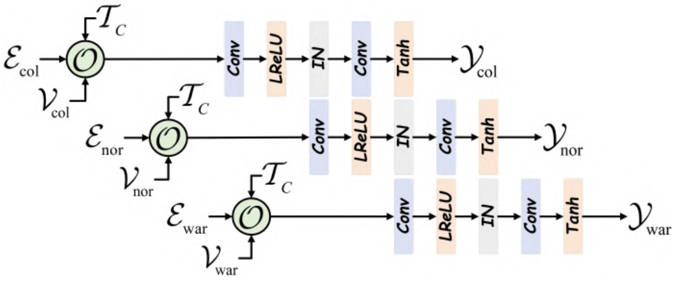
$\mathcal{T}_C$
$\mathcal{E}_{\text{col}}$
$\mathcal{V}_{\text{col}}$
$\mathcal{E}_{\text{nor}}$
$\mathcal{V}_{\text{nor}}$
$\mathcal{E}_{\text{war}}$
$\mathcal{V}_{\text{war}}$
$\mathcal{O}$
Conv
LReLU
IN
Conv
Tanh
$\mathcal{Y}_{\text{col}}$
$\mathcal{Y}_{\text{nor}}$
$\mathcal{Y}_{\text{war}}$

Fig. 10. Indication of three CNN-based multi-feature fusion networks. Conv denotes the convolutional layer. LReLU, Sigmoid and Tanh represent the leaky ReLU, sigmoid and tanh functions, IN is the instance normalization, $\mathcal{O}$ means the concatenation.

$\mathcal{V}$, the detail enhancement feature $\mathcal{E}$ and six channels $\mathcal{T}_c$ through three multi-feature fusion networks, as follows,

$$\begin{aligned}
\mathcal{Y}_{\text{col}} &= \mathcal{F}^{\text{col}}_{\text{fea}}(\mathcal{O}(\mathcal{V}_{\text{col}}, \mathcal{E}_{\text{col}}, \mathcal{T}_c)),\\
\mathcal{Y}_{\text{nor}} &= \mathcal{F}^{\text{nor}}_{\text{fea}}(\mathcal{O}(\mathcal{V}_{\text{nor}}, \mathcal{E}_{\text{nor}}, \mathcal{T}_c)),\\
\mathcal{Y}_{\text{war}} &= \mathcal{F}^{\text{war}}_{\text{fea}}(\mathcal{O}(\mathcal{V}_{\text{war}}, \mathcal{E}_{\text{war}}, \mathcal{T}_c)),
\end{aligned} \tag{17}$$

where $\mathcal{O}$ denotes concat operation, $\mathcal{Y}_{\text{col}}$, $\mathcal{Y}_{\text{nor}}$ and $\mathcal{Y}_{\text{war}}$ are three different tone enhanced results. We use three CNN-based multi-feature fusion networks ($\mathcal{F}^{\text{col}}_{\text{fea}}$, $\mathcal{F}^{\text{nor}}_{\text{fea}}$, $\mathcal{F}^{\text{war}}_{\text{fea}}$) to fuse the features and generate the final enhanced results of three different tones ($\mathcal{Y}_{\text{col}}$: the final results for the cold tone, $\mathcal{Y}_{\text{nor}}$: the final results for the normal tone and $\mathcal{Y}_{\text{war}}$: the final results for the warm tone). In Fig. 10, these three CNN-based multi-feature fusion networks can adaptive combine the detail results ($\mathcal{E}_{\text{col}}$, $\mathcal{E}_{\text{nor}}$, $\mathcal{E}_{\text{war}}$), color correction results ($\mathcal{V}_{\text{col}}$, $\mathcal{V}_{\text{nor}}$, $\mathcal{V}_{\text{war}}$), of three tones with 6D base channels $\mathcal{T}_c$. Fig. 11 shows the final results with different tones in the UIEB dataset [9].

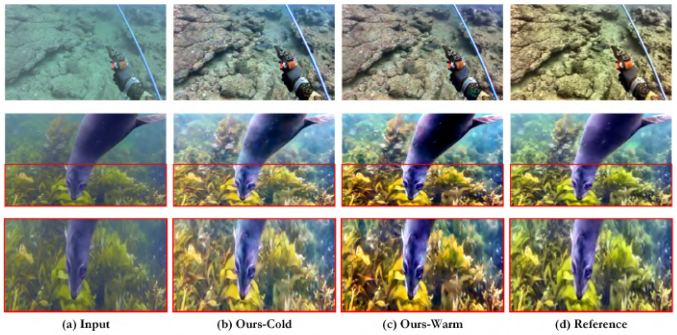
(a) Input (b) Ours-Cold (c) Ours-Warm (d) Reference

Fig. 11. Visual comparison of the cold tone results, the warm tone results and the reference results in the UIEB dataset. (a) input image, (b) ours-cold, (c) ours-warm and (d) reference image.

IV. Experiments

Implementation Details The proposed MM-UIE is trained with AdamW optimizer for 180 epochs. The initial learning rate is set to 0.0001, and then halved after every 30 epochs. The batch size is set as 4. All training images have been cropped to 224 × 224 patches, and then normalize to range $[0, 1]$. The experiments are implemented with Pytorch platform on two RTX3090 GPUs.

Datasets The UIEB [9] and SQUID [44] datasets are two commonly used UIE benchmark sets. There are 950 real underwater images included in the UIEB dataset, which has been collected from the Internet. As ground truths, the author manually selects images with better visual results following the processing of different algorithms. To obtain ground truth (GT), different enhancement algorithms are implemented and then image with better visual quality are manually selected as GTs. As for the SQUID dataset, 57 pairs of stereo images are included in the database, two of which are located in the Red Sea (representing tropical waters) and two in the Mediterranean Sea (representing temperate waters). This dataset does not contain GTs.

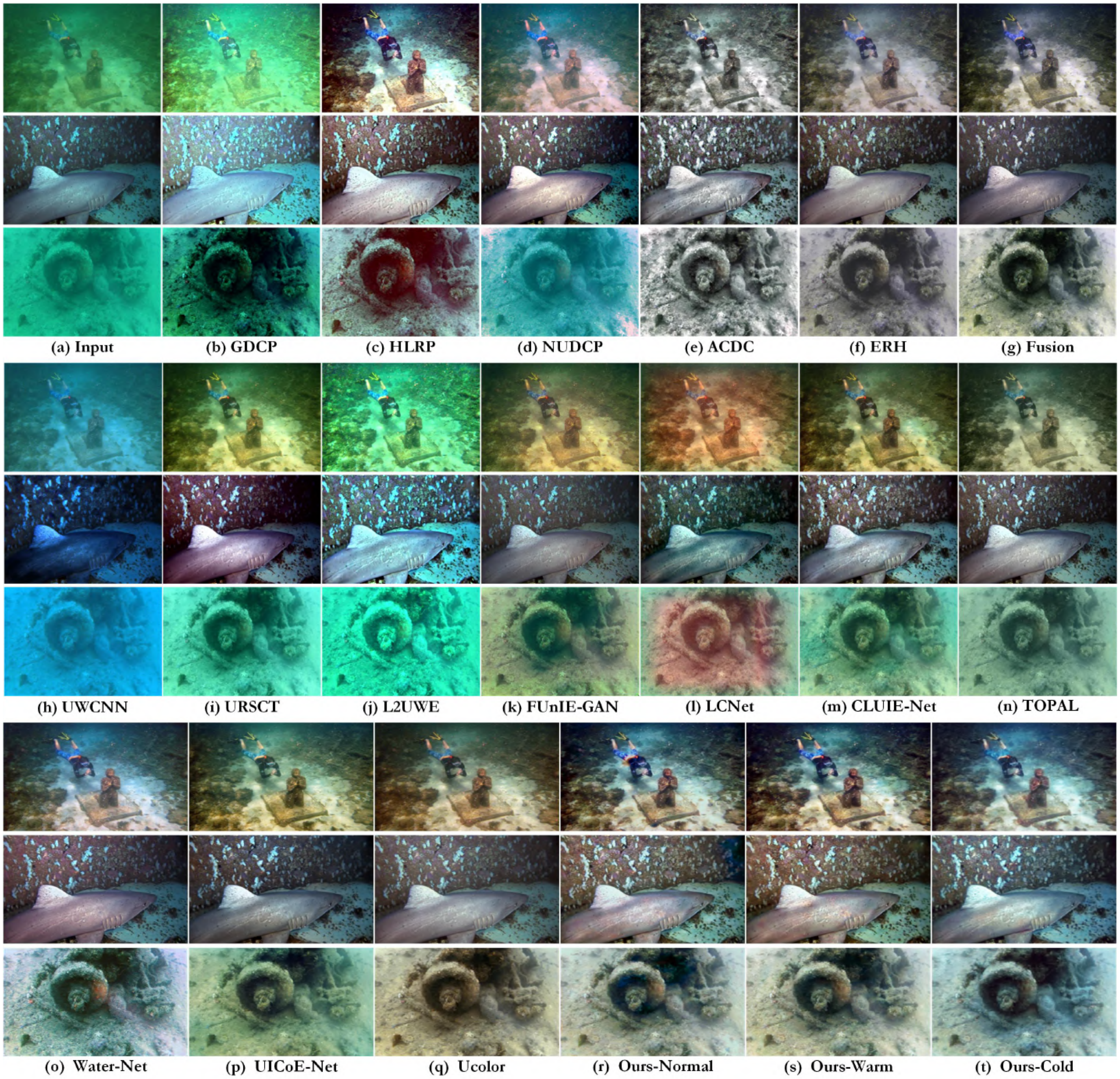
(a) Input (b) GDCP (c) HLRP (d) NUDCP (e) ACDC (f) ERH (g) Fusion

(h) UWCNN (i) URSCT (j) L2UWE (k) FUnIE-GAN (l) LCNet (m) CLUIE-Net (n) TOPAL

(o) Water-Net (p) UICoE-Net (q) Ucolor (r) Ours-Normal (s) Ours-Warm (t) Ours-Cold

Fig. 12. Visual comparison of UIEB-100 testset. (a) input image, (b) GDCP [35], (c) HLRP [15], (d) NUDCP [14], (e) ACDC [36], (f) ERH [37], (g) Fusion [12], (h) UWCNN [26], (i) URSCT [38], (j) L2UWE [39], (k) FUnIE-GAN [23], (l) LCNet [40], (m) CLUIE-Net [41], (n) TOPAL [42], (0) Water-Net [9], (p) UICoE-Net [43], (q) Ucolor [10], (r) ours-normal, (s) ours-warm and (t) ours-cold.

We first perform data augmentation on the UIEB dataset by using horizontal and vertical flipping and rotation at angles of $A \in [0, \pi/2, \pi, 3\pi/2]$. A total of 12680 training samples are obtained after augmentation. We select 990 images for testing, and remaining samples are used for training. Among the 990 test images, 100 images with severe degradation are specifically selected to conduct a difficult UIEB-100 testset, and the other 890 images make up an UIEB-890 testset. In addition, 100 images are extracted from SQUID dataset for the cross-dataset testing, namely SQUID-100 testset.

Metrics For full-reference evaluation, we use five commonly used metrics, i.e., MSE, RMSE, PSNR, SSIM and LPIPS [45]. These full reference indicators evaluate the distance between the image and the ground truth, which can measure the distortions. For no-reference indicators, we used another five assessments, i.e., PI [46], MA [47], NIQE [48], UCIQE [49], UIQM [50]. Compared with distortion measurements, these indicators focus on visual quality, contrast, and color level of images. Among them, UCIQE and UIQM are two unique indicators for underwater images, which can comprehensively evaluate enhanced underwater images.

Comparison Methods In order to verify the effectiveness of the proposed method, 16 UIE methods are selected for comparisons, including 6 traditional algorithms of GDCP [35],

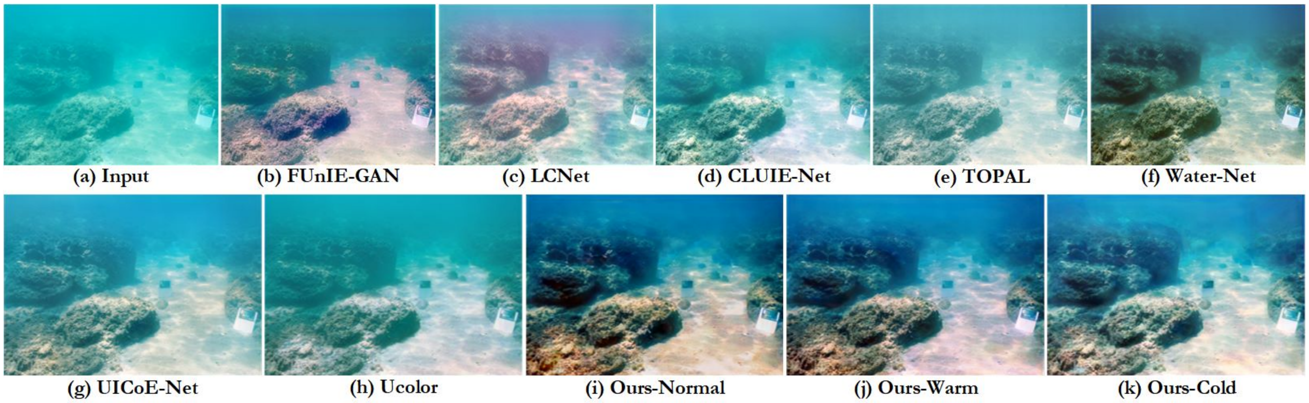

Fig. 13. Visual comparison of SQUID-100 testset. (a) input image, (b) FUnIE-GAN [23], (c) LCNet [40], (d) CLUIE-Net [41], (e) TOPAL [42], (f) Water-Net [9], (g) UICoE-Net [43], (h) Ucolor [10], (i) ours-normal, (j) ours-warm and (k) ours-cold.

TABLE II
EVALUATIONS OF DIFFERENT METHODS ON UIEB-890 TESTSET IN TERMS OF FULL-REFERENCE (MSE, RMSE, PSNR, SSIM, LPIPS) AND NO-REFERENCE (PI, MA, NIQE, UCIQE, UIQM) METRICS. RED, BLUE AND UNDERSCORED BOLD FONTS INDICATE THE BEST THREE RESULTS.

Method	Full-Reference					No-Reference				
	MSE↓	RMSE↓	PSNR↑	SSIM↑	LPIPS↓	PI↓	MA↑	NIQE↓	UCIQE↑	UIQM↑
FUnIE-GAN	242.9328	15.5863	23.7391	0.8751	0.2838	3.7993	7.6478	5.2463	0.5620	1.4063
LCNet	344.4753	18.5600	23.6221	0.9069	0.2207	3.4458	7.7556	4.6472	0.5738	1.4319
CLUIE-Net	389.2661	19.7298	24.4310	**0.9436**	0.1453	**3.1038**	**8.2809**	4.4885	0.5974	1.4355
TOPAL	387.3276	19.6806	24.2523	0.9064	0.1716	**3.1667**	**8.1648**	4.4983	0.5794	1.4036
Water-Net	548.4220	23.4184	22.5334	0.8581	0.3074	3.5524	7.7097	4.8144	0.6029	1.4164
UICoE-Net	294.1896	17.1520	24.1768	0.9188	0.1662	3.6122	7.6844	4.9088	0.5917	1.4263
Ucolor	225.4618	15.0154	25.8397	0.9174	0.1456	3.4851	7.5607	4.5310	0.5726	1.3558
Ours-Normal	**75.9174**	**8.7130**	**29.9073**	0.9169	**0.1310**	3.2671	7.9354	**4.4697**	**0.6109**	**1.4556**
Ours-Warm	**64.9680**	**8.0602**	**30.6512**	**0.9197**	**0.1215**	3.2045	**7.9646**	**4.3736**	**0.6114**	**1.4499**
Ours-Cold	**66.4712**	**8.1529**	**30.5979**	**0.9202**	**0.1218**	**3.2016**	7.9598	**4.3630**	**0.6117**	**1.4448**

HLRP [15], NUDCP [14], ACDC [36], ERH [37], and Fusion [12], and 10 SOTA learning-based models of UWCNN [26], URSCT [38], L2UWE [39], FUnIE-GAN [23], LCNet [40], CLUIE-Net [41], TOPAL [42], Water-Net [9], UICoE-Net [43], and Ucolor [10].

TABLE III
EVALUATIONS OF DIFFERENT METHODS ON UIEB-100 TESTSET IN TERMS OF FULL-REFERENCE (PSNR, SSIM) AND NO-REFERENCE (UCIQE, UIQM) METRICS. RED, BLUE AND UNDERSCORED BOLD FONTS INDICATE THE BEST THREE RESULTS.

Method	Full-Reference		No-Reference	
	PSNR↑	SSIM↑	UCIQE↑	UIQM↑
GDCP	12.6871	0.5256	0.5889	**1.5023**
HLRP	13.4891	0.2741	0.5629	**1.5218**
NUDCP	15.8837	0.6915	0.5891	1.4419
ACDC	18.1247	0.7016	0.5635	**1.5391**
ERH	19.2439	0.6929	0.5529	1.4781
Fusion	20.3664	0.8180	0.5925	1.4971
UWCNN	14.0549	0.4947	0.4930	1.3961
URSCT	14.1659	0.4623	0.5789	1.4200
L2UWE	14.1710	0.6892	0.5518	1.4865
FUnIE-GAN	18.1488	0.6509	0.5531	1.4324
LCNet	18.8990	0.7154	0.5588	1.4316
CLUIE-Net	20.5229	0.8021	0.5864	1.4548
TOPAL	21.1428	0.8142	0.5710	1.4282
Water-Net	21.5394	0.8223	0.5904	1.4319
UICoE-Net	21.6395	0.8472	0.5880	1.4607
Ucolor	21.6671	0.8411	0.5635	1.4168
Ours-Normal	**24.9131**	**0.8886**	**0.6043**	1.4968
Ours-Warm	**25.5133**	**0.9065**	**0.6074**	1.4876
Ours-Cold	**25.7043**	**0.9069**	**0.6057**	1.4913

TABLE IV
EVALUATIONS OF DIFFERENT METHODS ON SQUID-100 TESTSET IN TERMS OF NO-REFERENCE (UCIQE, UIQM) METRICS. RED, BLUE AND UNDERSCORED BOLD FONTS INDICATE THE BEST THREE RESULTS.

Method	No-Reference	
	UCIQE↑	UIQM↑
FUnIE-GAN	0.5359	**1.0584**
LCNet	0.5254	1.0034
CLUIE-Net	0.5099	0.9689
TOPAL	0.5131	0.9346
Water-Net	0.5621	0.9747
UICoE-Net	0.5267	1.0014
Ucolor	0.5035	0.8974
Ours-Normal	**0.5845**	**1.1315**
Ours-Warm	**0.5654**	**1.0762**
Ours-Cold	**0.5672**	1.0574

A. *Qualitative Evaluation*

The subjective results of these method on UIEB-100 and SQUID-100 testsets are illustrated in Fig. 12 and Fig. 13, respectively. Form these figures, we can obtain the following observations. Firstly, traditional algorithms can improve color degradation, resulting in enhanced results without obvious greenish or bluish colors. However, these processed images often suffer from monotonous colors and severe noise in the details. The GDCP and NUDCP algorithms have made some improvements in brightness, but they tend to produce uneven fogging phenomena and color distortion. The ACDC algorithm produces grayish white images with poor visual effects. The

HLRP algorithm tends to overexpose the images, while the ERH and Fusion algorithms produce darker results. In terms of learning-based methods, most of them exhibit better color and well-processed details compared to traditional methods. However, their results still contain some limitations. URSCT and L2UWE struggle to handle severe color cast. FUnIE-GAN and LCNet tend to introduce red color cast to the enhanced image, with LCNet exhibiting severe red artifacts. CLUIE-Net, TOPAL, and UICoE-Net still exhibit some color degradation in certain results. In contrast, our proposed MM-UIE not only achieves good results on the UIEB-100 and SQUID-100 test sets but also provides users with enhanced results in three different tones.

B. Quantitative Evaluation

In this subsection, we will compare our MM-UIE and SOTA methods quantitatively. Tab. III shows that we evaluate UIEB-100 using four metrics: PSNR, SSIM, UCIQE, and UIQM. Accordingly, the method proposed in this article has advantages in terms of PSNR, SSIM, and UCIQE metrics. Additionally, Tab. II shows some excellent algorithms tested on UIEB-890. This test is more comprehensive and specific, showing clearly the MM-UIE characteristics. In Tab. IV, eight of the ten metrics of MM-UIE exceed other algorithms. According to the SQUID-100 test set, our proposed method still has significant advantages over excellent algorithms in terms of both UCIQE and UIQM metrics. Overall, the MM-UIE proposed in this article performs well in nearly ten metrics across three datasets, with improved color performance and enhanced image quality.

TABLE V

ABLATION STUDY ON UIEB-100 TESTSET IN TERMS OF FULL-REFERENCE (PSNR, SSIM) AND NO-REFERENCE (UCIQE, UIQM) METRICS. BOLD FONTS INDICATE THE BEST RESULTS.THREE PIECES OF DATA CORRESPOND TO NORMAL, WARM AND COLD TONE RESULTS.

Method	Full-Reference		No-Reference	
	PSNR↑	SSIM↑	UCIQE↑	UIQM↑
3D Col. Ope.	23.5425	0.8511	0.5998	1.4872
w/o 6D Col. Ope.	21.8979	0.7989	0.5902	1.4734
w/o Warm Sup.	20.7406	0.7570	0.5759	1.4483
w/o Cold Sup.	20.9705	0.7795	0.5763	1.4443
Ours-Normal	**24.9131**	**0.8886**	**0.6043**	**1.4968**
3D Col. Ope.	24.2124	0.8680	0.6045	1.4788
w/o 6D Col. Ope.	22.8625	0.8275	0.6041	1.4767
w/o Warm Sup.	22.2889	0.8115	0.6005	1.4596
w/o Cold Sup.	21.6017	0.7898	0.5974	1.4768
Ours-Warm	**25.5133**	**0.9065**	**0.6074**	**1.4876**
3D Col. Ope.	23.5425	0.8511	0.5998	1.4872
w/o 6D Col. Ope.	21.8979	0.7989	0.5902	1.4734
w/o Warm Sup.	20.7406	0.7570	0.5759	1.4483
w/o Cold Sup.	20.9705	0.7795	0.5763	1.4443
Ours-Cold	**25.7043**	**0.9069**	**0.6057**	**1.4913**

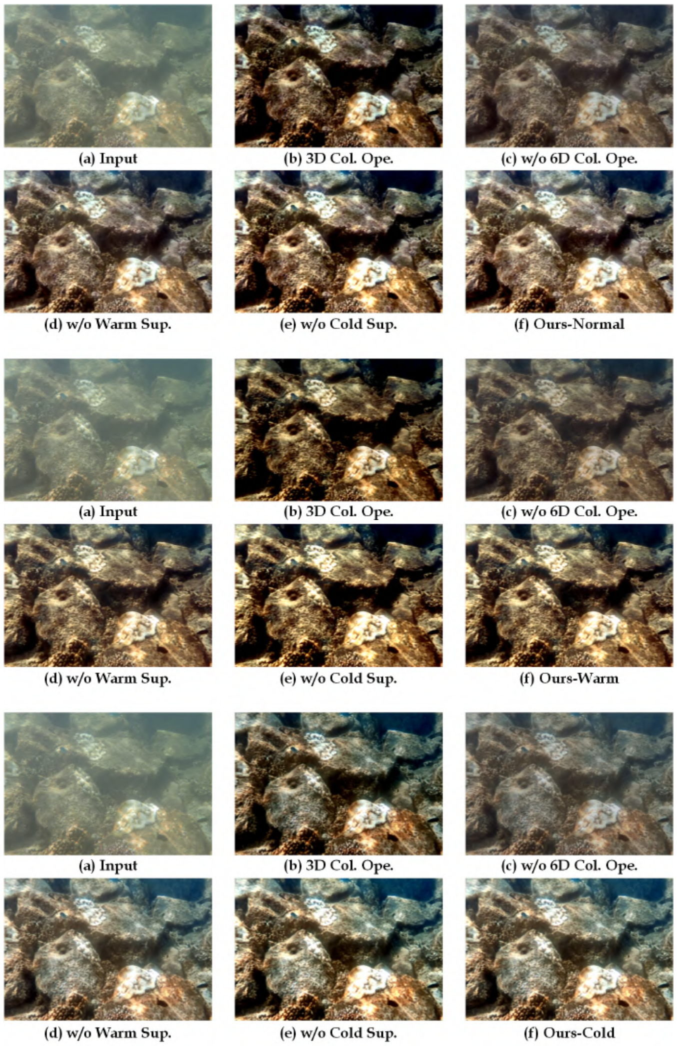
(a) Input
(b) 3D Col. Ope.
(c) w/o 6D Col. Ope.
(d) w/o Warm Sup.
(e) w/o Cold Sup.
(f) Ours-Normal
(a) Input
(b) 3D Col. Ope.
(c) w/o 6D Col. Ope.
(d) w/o Warm Sup.
(e) w/o Cold Sup.
(f) Ours-Warm
(a) Input
(b) 3D Col. Ope.
(c) w/o 6D Col. Ope.
(d) w/o Warm Sup.
(e) w/o Cold Sup.
(f) Ours-Cold

Fig. 14. Visual comparison of the ablation study. Three pieces of figure correspond to normal, warm and cold tone ablation study results. (a) input image, (b) with 3D color operator, (c) without 6D color operator, (d) without warm information supervision, (e) without cold information supervision and (f) normal/warm/cold tone results.

C. Ablation Study

An ablation experiment was designed to demonstrate the efficacy of the multi-modal information supervision and 6D color operator proposed in this paper. Tab. V and Fig. 14 show ablation results, w/o means without. Firstly, we can observe through w/o warm supervision and w/o cold supervision that there is a significant improvement in warm or cold tone results directly supervised by multimodal information compared to none, and it can affect normal tone image quality. The 6D color operators of normal tone results also contain information about warm and cold tone. Indirect explanation of multimodal information supervision can control image tone and improve image quality. Additionally, we can observe that the use of w/o 6D color operator results in a certain decrease in the effect. In contrast, the use of 3D color operator is not as effective as 6D color operator, indicating that 6D color operator has a significant effect on image color adjustment.

V. CONCLUSION

This paper proposed a novel framework for personalized underwater image enhancement with different tones. The proposed model consists of two stages, i.e., color enhancement, and detail enhancement. For color enhancement, a multi-modal supervised 6D color operator is presented. By using text information and multi-modal interactive learning, the proposed method can control the tone of enhanced image, and can learn to generate different tones through the same ground truth without tone information. Experimental results demonstrate that the proposed method can outperform SOTA methods in both subjective and objective evaluation.

In summary, it has been shown that the method we propose can generate enhancement results of different tones in accordance with individual preferences, which can satisfy the needs of groups of people who like cold tones, warm tones, and have no preference for tones. However, the perception of color is also influenced by their emotions. People tend to prefer warm colors when they are passionate, and cool colors when they are calm. As our method cannot detect the emotions of the viewer, we are unable to change the enhancement results of different tones as necessary. A future project aims to design an interactive system that adapts to the emotional changes of the viewer and provides more accurate enhancement results in response.

References

[1] R. Schettini and S. Corchs, “Underwater image processing: state of the art of restoration and image enhancement methods,” *EURASIP journal on advances in signal processing*, vol. 2010, pp. 1–14, 2010. 1

[2] M. Jian, X. Liu, H. Luo, X. Lu, H. Yu, and J. Dong, “Underwater image processing and analysis: A review,” *Signal Processing: Image Communication*, vol. 91, p. 116088, 2021. 1

[3] S. Raveendran, M. D. Patil, and G. K. Birajdar, “Underwater image enhancement: a comprehensive review, recent trends, challenges and applications,” *Artificial Intelligence Review*, vol. 54, pp. 5413–5467, 2021. 1

[4] S. Luria and J. A. S. Kinney, “Underwater vision: The physical and psychological bases of the visual distortions that occur underwater are discussed.” *Science*, vol. 167, no. 3924, pp. 1454–1461, 1970. 1

[5] C. Zhang, J. Su, Y. Ju, K.-M. Lam, and Q. Wang, “Efficient inductive vision transformer for oriented object detection in remote sensing imagery,” *IEEE Transactions on Geoscience and Remote Sensing*, vol. 61, 2023. 1

[6] C. Zhang, K.-M. Lam, T. Liu, Y.-L. Chan, and Q. Wang, “Structured adversarial self-supervised learning for robust object detection in remote sensing images,” *IEEE Transactions on Geoscience and Remote Sensing*, vol. 62, 2024. 1

[7] Z. Zhang, H. Zheng, R. Hong, M. Xu, S. Yan, and M. Wang, “Deep color consistent network for low-light image enhancement,” in *Proceedings of the IEEE/CVF conference on computer vision and pattern recognition*, 2022, pp. 1899–1908. 1

[8] K. Chi, Y. Yuan, and Q. Wang, “Trinity-net: Gradient-guided swin transformer-based remote sensing image dehazing and beyond,” *IEEE Transactions on Geoscience and Remote Sensing*, vol. 61, pp. 1–14, 2023. 1

[9] C. Li, C. Guo, W. Ren, R. Cong, J. Hou, S. Kwong, and D. Tao, “An underwater image enhancement benchmark dataset and beyond,” *IEEE Transactions on Image Processing*, vol. 29, pp. 4376–4389, 2019. 1, 3, 6, 7, 8

[10] C. Li, S. Anwar, J. Hou, R. Cong, C. Guo, and W. Ren, “Underwater image enhancement via medium transmission-guided multi-color space embedding,” *IEEE Transactions on Image Processing*, vol. 30, pp. 4985–5000, 2021. 1, 3, 4, 7, 8

[11] R. Liu, Z. Jiang, S. Yang, and X. Fan, “Twin adversarial contrastive learning for underwater image enhancement and beyond,” *IEEE Transactions on Image Processing*, vol. 31, pp. 4922–4936, 2022. 1, 3

[12] C. O. Ancuti, C. Ancuti, C. De Vleeschouwer, and P. Bekaert, “Color balance and fusion for underwater image enhancement,” *IEEE Transactions on image processing*, vol. 27, no. 1, pp. 379–393, 2017. 3, 7, 8

[13] W. Zhang, P. Zhuang, H.-H. Sun, G. Li, S. Kwong, and C. Li, “Underwater image enhancement via minimal color loss and locally adaptive contrast enhancement,” *IEEE Transactions on Image Processing*, vol. 31, pp. 3997–4010, 2022. 3

[14] W. Song, Y. Wang, D. Huang, A. Liotta, and C. Perra, “Enhancement of underwater images with statistical model of background light and optimization of transmission map,” *IEEE Transactions on Broadcasting*, vol. 66, no. 1, pp. 153–169, 2020. 3, 7, 8

[15] P. Zhuang, J. Wu, F. Porikli, and C. Li, “Underwater image enhancement with hyper-laplacian reflectance priors,” *IEEE Transactions on Image Processing*, vol. 31, pp. 5442–5455, 2022. 3, 7, 8

[16] L. Shen, M. Reda, X. Zhang, Y. Zhao, and S. G. Kong, “Polarization-driven solution for mitigating scattering and uneven illumination in underwater imagery,” *IEEE Transactions on Geoscience and Remote Sensing*, vol. 62, pp. 1–15, 2024. 3

[17] H. Wang, W. Zhang, L. Bai, and P. Ren, “Metalantis: A comprehensive underwater image enhancement framework,” *IEEE Transactions on Geoscience and Remote Sensing*, vol. 62, pp. 1–19, 2024. 3

[18] D. Liang, J. Chu, Y. Cui, Z. Zhai, and D. Wang, “Npt-ul: An underwater image enhancement framework based on nonphysical transformation and unsupervised learning,” *IEEE Transactions on Geoscience and Remote Sensing*, vol. 62, pp. 1–19, 2024. 3

[19] J. Yin, Y. Wang, B. Guan, X. Zeng, and L. Guo, “Unsupervised underwater image enhancement based on disentangled representations via double-order contrastive loss,” *IEEE Transactions on Geoscience and Remote Sensing*, vol. 62, pp. 1–15, 2024. 3

[20] J. Zhou, Q. Gai, D. Zhang, K.-M. Lam, W. Zhang, and X. Fu, “Iacc: Cross-illumination awareness and color correction for underwater images under mixed natural and artificial lighting,” *IEEE Transactions on Geoscience and Remote Sensing*, vol. 62, pp. 1–15, 2024. 3

[21] M. Yu, L. Shen, Z. Wang, and X. Hua, “Task-friendly underwater image enhancement for machine vision applications,” *IEEE Transactions on Geoscience and Remote Sensing*, vol. 62, pp. 1–14, 2024. 3

[22] Q. Jiang, Y. Zhang, F. Bao, X. Zhao, C. Zhang, and P. Liu, “Two-step domain adaptation for underwater image enhancement,” *Pattern Recognition*, vol. 122, p. 108324, 2022. 3

[23] M. J. Islam, Y. Xia, and J. Sattar, “Fast underwater image enhancement for improved visual perception,” *IEEE Robotics and Automation Letters*, vol. 5, no. 2, pp. 3227–3234, 2020. 3, 7, 8

[24] X. Liu, S. Lin, and Z. Tao, “Learning multiscale pipeline gated fusion for underwater image enhancement,” *Multimedia Tools and Applications*, pp. 1–24, 2023. 3

[25] L. Peng, C. Zhu, and L. Bian, “U-shape transformer for underwater image enhancement,” *IEEE Transactions on Image Processing*, 2023. 3

[26] C. Li, S. Anwar, and F. Porikli, “Underwater scene prior inspired deep underwater image and video enhancement,” *Pattern Recognition*, vol. 98, p. 107038, 2020. 3, 7, 8

[27] L. Shen, H. Xia, X. Zhang, Y. Zhao, N. Li, S. G. Kong, B. Wang, and Z. Li, “U^{2}pnet: An unsupervised underwater image-restoration network using polarization,” *IEEE Transactions on Cybernetics*, vol. 54, no. 9, pp. 5164–5177, 2024. 3

[28] A. Radford, J. W. Kim, C. Hallacy, A. Ramesh, G. Goh, S. Agarwal, G. Sastry, A. Askell, P. Mishkin, J. Clark *et al.*, “Learning transferable visual models from natural language supervision,” in *International conference on machine learning*. PMLR, 2021, pp. 8748–8763. 3

[29] S. Yang, M. Ding, Y. Wu, Z. Li, and J. Zhang, “Implicit neural representation for cooperative low-light image enhancement,” *arXiv preprint arXiv:2303.11722*, 2023. 3

[30] C. Ju, T. Han, K. Zheng, Y. Zhang, and W. Xie, “Prompting visual-language models for efficient video understanding,” in *European Conference on Computer Vision*. Springer, 2022, pp. 105–124. 3

[31] Z. Liang, C. Li, S. Zhou, R. Feng, and C. C. Loy, “Iterative prompt learning for unsupervised backlit image enhancement,” in *Proceedings of the IEEE/CVF International Conference on Computer Vision*, 2023, pp. 8094–8103. 3

[32] J. Wang, K. C. Chan, and C. C. Loy, “Exploring clip for assessing the look and feel of images,” in *Proceedings of the AAAI Conference on Artificial Intelligence*, vol. 37, no. 2, 2023, pp. 2555–2563. 4

[33] Z. Zheng, W. Ren, X. Cao, X. Hu, T. Wang, F. Song, and X. Jia, “Ultra-high-definition image dehazing via multi-guided bilateral learning,” in *2021 IEEE/CVF Conference on Computer Vision and Pattern Recognition (CVPR)*, 2021, pp. 16 180–16 189. 4

[34] X. Liu, S. Lin, K. Chi, Z. Tao, and Y. Zhao, “Boths: Super lightweight network-enabled underwater image enhancement,” *IEEE Geoscience and Remote Sensing Letters*, vol. 20, pp. 1–5, 2022. 5

[35] Y.-T. Peng, K. Cao, and P. C. Cosman, “Generalization of the dark channel prior for single image restoration,” *IEEE Transactions on Image Processing*, vol. 27, no. 6, pp. 2856–2868, 2018. 7

[36] W. Zhang, Y. Wang, and C. Li, “Underwater image enhancement by attenuated color channel correction and detail preserved contrast enhancement,” *IEEE Journal of Oceanic Engineering*, vol. 47, no. 3, pp. 718–735, 2022. 7, 8

[37] H. Song, L. Chang, Z. Chen, and P. Ren, “Enhancement-registration-homogenization (erh): A comprehensive underwater visual reconstruc-

tion paradigm," *IEEE transactions on pattern analysis and machine intelligence*, vol. 44, no. 10, pp. 6953–6967, 2021. 7, 8

[38] T. Ren, H. Xu, G. Jiang, M. Yu, X. Zhang, B. Wang, and T. Luo, "Reinforced swin-convs transformer for simultaneous underwater sensing scene image enhancement and super-resolution," *IEEE Transactions on Geoscience and Remote Sensing*, vol. 60, pp. 1–16, 2022. 7, 8

[39] T. P. Marques and A. B. Albu, "L2uwe: A framework for the efficient enhancement of low-light underwater images using local contrast and multi-scale fusion," in *Proceedings of the IEEE/CVF conference on computer vision and pattern recognition workshops*, 2020, pp. 538–539. 7, 8

[40] N. Jiang, W. Chen, Y. Lin, T. Zhao, and C.-W. Lin, "Underwater image enhancement with lightweight cascaded network," *IEEE transactions on multimedia*, vol. 24, pp. 4301–4313, 2021. 7, 8

[41] K. Li, L. Wu, Q. Qi, W. Liu, X. Gao, L. Zhou, and D. Song, "Beyond single reference for training: underwater image enhancement via comparative learning," *IEEE Transactions on Circuits and Systems for Video Technology*, 2022. 7, 8

[42] Z. Jiang, Z. Li, S. Yang, X. Fan, and R. Liu, "Target oriented perceptual adversarial fusion network for underwater image enhancement," *IEEE Transactions on Circuits and Systems for Video Technology*, vol. 32, no. 10, pp. 6584–6598, 2022. 7, 8

[43] Q. Qi, Y. Zhang, F. Tian, Q. J. Wu, K. Li, X. Luan, and D. Song, "Underwater image co-enhancement with correlation feature matching and joint learning," *IEEE Transactions on Circuits and Systems for Video Technology*, vol. 32, no. 3, pp. 1133–1147, 2021. 7, 8

[44] D. Berman, D. Levy, S. Avidan, and T. Treibitz, "Underwater single image color restoration using haze-lines and a new quantitative dataset," *IEEE transactions on pattern analysis and machine intelligence*, vol. 43, no. 8, pp. 2822–2837, 2020. 6

[45] R. Zhang, P. Isola, A. A. Efros, E. Shechtman, and O. Wang, "The unreasonable effectiveness of deep features as a perceptual metric," in *Proceedings of the IEEE conference on computer vision and pattern recognition*, 2018, pp. 586–595. 7

[46] Y. Blau, R. Mechrez, R. Timofte, T. Michaeli, and L. Zelnik-Manor, "The pirm challenge on perceptual super resolution," 2018. 7

[47] C. Ma, C.-Y. Yang, X. Yang, and M.-H. Yang, "Learning a no-reference quality metric for single-image super-resolution," *Computer Vision and Image Understanding*, vol. 158, pp. 1–16, 2017. 7

[48] A. Mittal, R. Soundararajan, and A. C. Bovik, "Making a "completely blind" image quality analyzer," *IEEE Signal processing letters*, vol. 20, no. 3, pp. 209–212, 2012. 7

[49] M. Yang and A. Sowmya, "An underwater color image quality evaluation metric," *IEEE Transactions on Image Processing*, vol. 24, no. 12, pp. 6062–6071, 2015. 7

[50] K. Panetta, C. Gao, and S. Agaian, "Human-visual-system-inspired underwater image quality measures," *IEEE Journal of Oceanic Engineering*, vol. 41, no. 3, pp. 541–551, 2016. 7

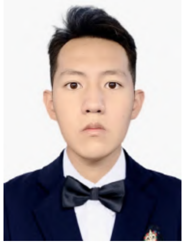

Xu Liu (S'21) is currently pursuing the M.E. degree in Information and Communication Engineering at the School of Computer Science and Information Engineering, Hefei University of Technology, Hefei, China. He received the B.E. degree in Electronic and Information Engineering, the B.E. degree in Data Science and Big Data Technology (Tencent Premier Class) from the Liaoning Technical University, Huludao, China, in 2022. His research interests include deep learning and computer vision.

Yang Zhao (M'16) received his B.E. and Ph.D. degrees from the Department of Automation, University of Science and Technology of China, in 2008 and 2013. From September 2013 to October 2015, he was a Postdoctoral Fellow with the School of Electronic and Computer Engineering, Peking University Shenzhen Graduate School, China. He is currently a research associate professor in the School of Computer and Information, Hefei University of Technology. His research interests include image processing and pattern recognition.

Kaichen Chi received the B.E. degree in electronic and information engineering and the M.E. degree in communication and information system from Liaoning Technical University, Huludao, China, in 2019 and 2022 respectively. He is currently working toward the Ph.D. degree in the School of Artificial Intelligence, Optics and Electronics (iOPEN), Northwestern Polytechnical University, Xi'an, China. His research interests include image processing and deep learning.

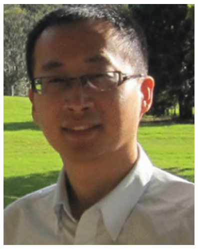

Zhao Zhang (SM'17) received the Ph.D. degree from the City University of Hong Kong, Hong Kong, in 2013. He is currently a Full Professor with the School of Computer and Information, Hefei University of Technology, Hefei, China. During his Ph.D., he visited the National University of Singapore, Singapore, where he worked with Prof. Shuicheng Yan, from February to May 2012. He also visited the Chinese Academy of Sciences, Beijing, China, where he worked with Prof. Cheng-Lin Liu, from September to December 2012. His research interests include machine learning, computer vision, and pattern recognition. He has authored or coauthored more than 130 technical papers published at prestigious journals and conferences, including 49 IJCV or IEEE/ACM Transactions papers, and 30 Top-tier conference papers such as CVPR, NeurIPS, ACM MM, ICLR, AAAI, and IJCAI, with Google Scholar citations more than 5,900 times and H-index 44. He was/is an Associate Editor for IEEE Transactions on Image Processing, Pattern Recognition, and Neural Networks. He is/has been a SPC Member/Area Chair of ACM MM, AAAI, IJCAI, SDM, and BMVC. He is a Distinguished Member of the CCF.

Yanxiang Chen received the B.Sc. and the M.Sc. degree in electronic information engineering from Hefei University of Technology, China in 1993 and 1996, and the Ph.D. degree in signal and information processing from University of Science and Technology of China, Hefei, China, in 2004. She has been a visiting scholar in University of Illinois at Urbana-Champaign from 2006 to 2008, and in National University of Singapore from 2012 to 2013. She is currently a professor in School of Computer Science and Information Engineering, Hefei University of Technology. Her research interests include multimodal signal processing, pattern recognition and machine learning.

Wei Jia (M'12) received the B.Sc. degree in informatics from Central China Normal University, Wuhan, China, in 1998, the M.Sc. degree in computer science from Hefei University of Technology, Hefei, China, in 2004, and the Ph.D. degree in pattern recognition and intelligence systems from the University of Science and Technology of China, Hefei, in 2008. He was a Research Assistant Professor and an Associate Professor with Hefei Institutes of Physical Science, Chinese Academy of Science, Beijing, China, from 2008 to 2016. He is currently a Professor with the School of Computer and Information, Hefei University of Technology. His research interests include computer vision, biometrics, pattern recognition, and image processing.